Scientia Iranica F (2013) 20(6), 2285–2296

SCIENTIA IRANICA

Sharif University of Technology
Scientia Iranica
Transaction F: Nanotechnology
www.scientiairanica.com

Optimal sliding mode control for atomic force microscope tip positioning during nano-manipulation process

H. Babahosseini[a], S.H. Mahboobi[b], M. Khorsand Vakilzadeh[c], A. Alasty[c] and A. Meghdari[c,*]

a. *Department of Mechanical Engineering, Virginia Tech, Blacksburg, VA, USA.*
b. *Department of Bioengineering, University of California, Berkeley, CA, USA.*
c. *Center of Excellence in Design, Robotics and Automation, School of Mechanical Engineering, Sharif University of Technology, Tehran, Iran.*

Received 21 June 2011; received in revised form 1 December 2012; accepted 21 January 2013

KEYWORDS
AFM-based nanomanipulation;
Nanoscale interaction forces;
Optimal nonlinear control.

Abstract. This research presents two-dimensional controlled pushing-based nanomanipulation using an Atomic Force Microscope (AFM). A reliable control of the AFM tip position is crucial to AFM-based manipulation since the tip can jump over the target nanoparticle causing the process to fail. However, detailed modeling and an understanding of the interaction forces on the AFM tip have a central role in this process. In the proposed model, the Lund-Grenoble (LuGre) method is used to model the dynamic friction force between the nanoparticle and the substrate. This model leads to the stick-slip behavior of the nanoparticle, which is in agreement with the experimental behavior at nanoscale. Derjaguin interaction force, which includes both attractive and repulsive interactions, is used to model the contact between the tip and nanoparticle. AFM is modeled by the lumped-parameter model. A controller is designed based on the proposed dynamic model for positioning of the AFM tip during a desired nanomanipulation task. An optimal sliding mode approach is used to design the controller, and the performance of the controller is shown by the simulation.

1. Introduction

Recently, the Atomic Force Microscope (AFM) has evolved into a promising tool for micro/nanoparticles manipulation and assembly [1]. A controlled AFM probe, as a pushing manipulator, is able to position the micro/nanoparticles in a two-dimensional space to build miniaturized structures [1,2]. A precise controller that guarantees a stable and accurate tip positioning, is essential for nanomanipulation.

Thus far, some control schemes have been designed to make the AFM tip track a certain trajectory for the manipulation task. Delnavaz et al. [1] proposed a combined classical and second order sliding mode for vibration suppression of the AFM tip in nanomanipulation tasks, while the AFM has been modeled by a mass-spring-damper system. In addition, Raifi et al. [3] established a robust adaptive controller for AFM tip positioning. In this reference, the proposed modeling includes the coupled dynamics of the microcantilever and piezotube actuator. Uncertainties due to the probe-sample contact are considered in the model.

In this paper, an optimal sliding mode approach is proposed to control the AFM probe as a nonlinear sys-

*. *Corresponding author. Tel.: +98 21 66165541; Fax:+98 21 66000021*
E-mail address: meghdari@sharif.edu (A. Meghdari)

tem. This approach displays a satisfactory performance and robustness to model uncertainties, while having a simple control structure. To obtain an optimal control response, slope tuning of the sliding mode surface, which is a complex task, is done by the LQ method [4].

During manipulation, the tip-particle-substrate system experiences complicated dynamics. A perfect model of nanomanipulation is crucial for a successful control, and, so far, several research studies have been conducted to model AFM-based nanomanipulation [5-9]. Most of these works have applied static friction models that have shortcomings and are not proper for nanoscale phenomena. Tafazzoli et al. [5-7] proposed a model of the AFM-based lateral nanomanipulation process. They used a traditional coulomb friction model with an additional modifying term as the nano-friction force. This friction force reproduces a steady sliding response of the nanoparticle, which is usually observed in the macroscale. The dynamic behavior of a nanoparticle during AFM-based pushing is studied in [10,11]. The model is composed of the LuGre frictional sub-model, which leads to the stick-slip behavior of the nanoparticle. Some studies have used molecular dynamics to investigate the behaviors of the nanoparticle during nanomanipulation [12,13].

The remainder of the paper is organized as follows. In Section 2, the nanomanipulation modeling is presented. A new sliding mode control approach, optimized by the Linear Quadratic (LQ) method, is introduced in Section 3 and an optimal nonlinear controller is designed to suppress the vibration of the AFM microcantilever and make the tip track the specified trajectory. Finally, simulation results are illustrated and the conclusion is drawn in Sections 4 and 5, respectively.

2. Nanomanipulation modeling

AFM-based nanomanipulation modeling can be divided into two subsystems: the AFM dynamic model and the dynamic model of the nanoparticle. Also, three important phenomena, including nanoscale interaction forces, contact mechanics, and nanoscale friction force, are coupled in the dynamical model. The following sections will be devoted to presenting a suitable model of the AFM and the nanoparticle during manipulation.

2.1. AFM model

The Atomic Force Microscope (AFM) system is a promising tool for nanomanipulation. The AFM provides additional capabilities and advantages compared to other manipulators; especially its ability to manipulate metallic nanoparticles in every environment. The AFM pushes the individual nanoparticle by exerting direct force on it in the desired direction. A typical AFM system consists of a piezoelectric actuator and a microcantilever chip with a sharp tip mounted on the piezoelectric. A position sensitive photo detector comes with the system, which receives a laser beam reflected from the end point of the microcantilever to provide its deflection feedback [14].

The current AFM model is based on a lumped-parameters modeling approach [5,15]. The AFM cantilever is modeled as a 3-Degree Of Freedom (DOFs) mass-spring system. The springs include a linear spring to account for the normal deflections and a torsional spring for the lateral twisting of the probe. The lateral deflection of the microcantilever is not considerable, so, it is ignored [5]. The microcantilever has Young's modulus, E, shear modulus, G, length, L, width, w, and thickness, t. The stiffness coefficients of the springs, k_θ and k_z, can be calculated as:

$$k_\theta = \frac{Ewt^3}{6L(1+\nu)}, \tag{1}$$

$$k_z = \frac{Ewt^3}{4L^3}. \tag{2}$$

The force (F_z) and moment (M_θ) of the springs are proportional to the vertical deformation (z_c) and the torsional angle (θ), respectively:

$$F_z = k_z.z_c, \tag{3}$$

$$M_\theta = k_\theta.\theta. \tag{4}$$

A rigid AFM tip is also attached to the microcantilever lumped model. Figure 1 depicts a free body diagram of the AFM lumped-parameters model. The spring force (F_z), moment (M_θ) and the tip/particle interaction force (F_{tp}) are illustrated in Figure 1.

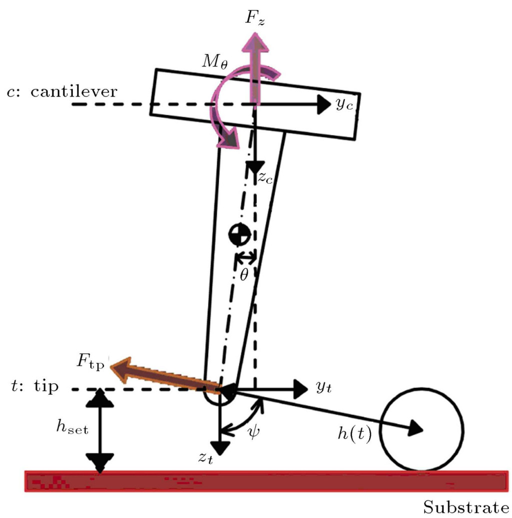

Figure 1. Free body diagram of the AFM lumped-parameters model during nanomanipulation.

In Figure 1, y_t and y_c are tip base and tip apex lateral movements. Besides, z_t and z_c are tip base and tip apex vertical movements, and θ is the tip torsional angle around the x axis. The selected local coordinates have the following kinematical relationships in y and z directions:

$$z_t = z_c + H' \cos\theta,$$

$$\dot{z}_t = \dot{z}_c - H'\dot{\theta}\sin\theta,$$

$$\ddot{z}_t = \ddot{z}_c - H'\ddot{\theta}\sin\theta - H'\dot{\theta}^2\cos\theta, \tag{5}$$

$$y_t = y_c - H'\sin\theta,$$

$$\dot{y}_t = V_{\text{stage}} - H'\dot{\theta}\cos\theta,$$

$$\ddot{y}_t = \ddot{y}_c - H'\ddot{\theta}\cos\theta + H'\dot{\theta}^2\sin\theta, \tag{6}$$

where V_{stage} is the probe stage constant velocity. The Ordinary Differential Equations (ODEs) of motion for the AFM in y and z directions, and the lateral twisting, θ, are as follows:

$$\sum \vec{F}_y = m\vec{a}_y,$$

$$-F_{\text{tp}}\sin\psi - F_y + u = m_t\ddot{y}_\otimes + m_c\ddot{y}_c,$$

$$= m_t\left(\frac{\ddot{y}_t + \ddot{y}_c}{2}\right) + m_c\ddot{y}_c, \tag{7}$$

$$\sum \vec{F}_z = m\vec{a}_z,$$

$$-F_{\text{tp}}\cos\psi - F_z = m_t\ddot{z}_\otimes + m_c\ddot{z}_c$$

$$= m_t\left(\frac{\ddot{z}_t + \ddot{z}_c}{2}\right) + m_c\ddot{z}_c, \tag{8}$$

$$\sum \vec{M}_c = I\ddot{\theta},$$

$$F_{\text{tp}}\cos\psi.H'\sin\theta + F_{\text{tp}}\sin\psi.H'\cos\theta - M_\theta$$

$$= I\ddot{\theta} = (I_t + I_c)\ddot{\theta}, \tag{9}$$

$$H' = H + \frac{t}{2}, \tag{10}$$

where u is the control input force which can be exerted on the microcantilever in the z direction by a piezo actuator located in the base of the microcantilever; m_c is the equivalent cantilever mass; I_c is the cantilever moment of inertia through the geometric center of the cantilever cross section (c); m_t is the tip effective mass, I_t is the inertia moment of the tip through point c, and H is the AFM tip height. F_{tp} is the tip/particle interaction force defined in the next section.

ψ, as illustrated in Figure 1, is the angle of F_{tp}, and is calculated as the following equation:

$$\psi = \tan^{-1}\left(\frac{D_{\text{set}} - y_t + y_p}{h_{\text{set}} - R_p + \delta_{\text{ps}}}\right). \tag{11}$$

$h(t)$ is the separation distance between the tip and the nanoparticle along the pushing direction and is obtained by:

$$h(t) = \sqrt{(D_{\text{set}} - y_t + y_p)^2 + (h_{\text{set}} - R_p + \delta_{\text{ps}})^2} + \delta_{\text{tp}} - (R_t + R_p). \tag{12}$$

In the above equations, D_{set} is the initial horizontal distance between the tip and particle centers, h_{set} is the desired height of the tip apex center from the substrate, and y_p is the total discrete movement of the particle in the manipulation direction. R_p and R_t are the particle and the tip apex radius, respectively. Finally, δ_{tp} and δ_{ps} are deformation depths in the tip/particle and the particle/substrate contact surfaces, which are discussed later. The subscript indicates that t is tip, p is particle and s is substrate.

2.2. Nanoscale interaction forces

There are different interaction forces dominant at the nanoscale, including capillary, electrostatic, van der Waals forces and repulsive forces [16]. Here, the Derjaguin potential function is applied for the nanoscale interactions, which represents both attractive and repulsive interactions between the AFM tip and the nanoparticle [16,17]. In this model, the van der Waals force is the sole attractive force between the tip and the particle for simplicity by assuming that the nanomanipulation process is performed in a clean vacuum cell and with a conductive grounding [18,19]. In addition to attractive force, the repulsive force is considered between the tip and the nanoparticle, which results in a contact deformation. The corresponding Derjaguin interaction force, F_{tp}, along the central line of the tip/particle is the negative partial derivative of the Derjaguin potential, V_{DMT} with respect to the separation distance, h, namely, $F_{\text{tp}} = -\frac{\partial}{\partial h}V_{\text{DMT}}$, and is given as [16,17]:

$$F_{\text{tp}}(h(t)) = \begin{cases} \frac{-\bar{H}_{\text{tp}}\tilde{R}}{6h(t)^2} \quad \text{for: } h(t) \geq a_0 \\ \frac{-\bar{H}_{\text{tp}}\tilde{R}}{6a_0^2} + \frac{4}{3}E^*\sqrt{\tilde{R}}(a_0 - h(t))^{\frac{3}{2}} \quad \text{for: } h(t) < a_0 \end{cases}$$

$$E^* = \left[\frac{(1-\nu_t)^2}{E_t} + \frac{(1-\nu_p)^2}{E_p}\right]^{-1}, \tag{13}$$

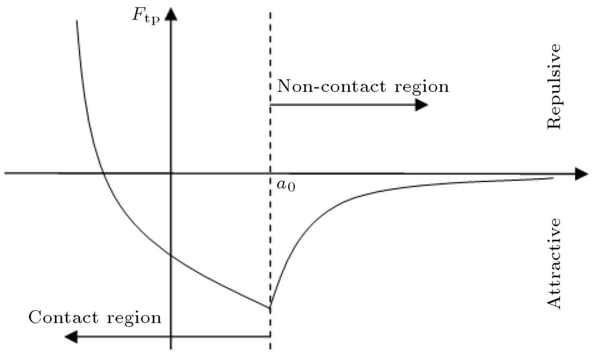

Figure 2. The profile of the Derjaguin interaction force [10]

$$\frac{1}{\tilde{R}} = \frac{1}{R_t} + \frac{1}{R_p}, \tag{14}$$

where a_0 is the interatomic separation distance introduced to avoid numerical divergence of F_{tp} as proposed in [10]. $\bar{H}$ is the Hamacker constant, E^* is the effective tip/particle elastic modulus, E_t and E_p are the Young's modulus of the tip and the particle, and ν_t and ν_p are the Poisson coefficient of the tip and the particle. $\tilde{R}$ is the effective tip/particle radius.

Figure 2 illustrates the profile of the Derjaguin interaction force, F_{tp}, versus separation distance, h. The negative value of F_{tp} demonstrates an attractive force, while the positive value indicates a repulsive force. Line $h = a_0$ indicates the boundary line between the contact and the non-contact region. The initial contact happens when the outset atoms of the tip and the nanoparticle touch each other.

2.3. Nanoparticle model

The nanoparticle is assumed to be an elastic spherical object. A free body diagram of the nanoparticle is depicted in Figure 3. During nanomanipulation, the nanoparticle experiences nano friction force, and

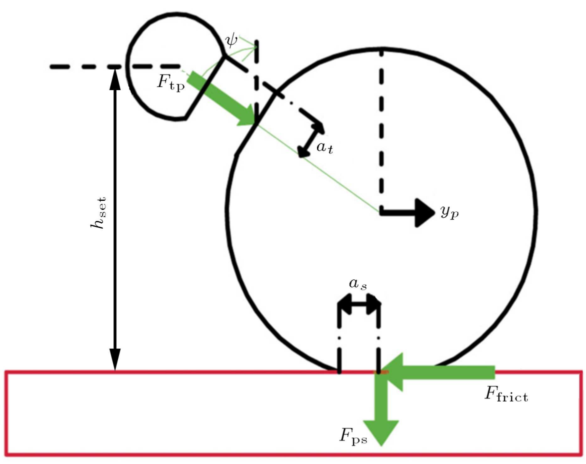

Figure 3. Free body diagram of the nanoparticle which experiences interaction forces and friction force during manipulation.

tip/particle and particle/substrate interaction forces. The equation of motion in the y direction and the balancing equation in the z direction for the nanoparticle are derived as follows:

$$F_{\text{tp}} \sin\psi - \text{sign}(\dot{y}_p) F_{\text{frict}} = m_p \ddot{y}_p(t), \tag{15}$$

$$F_{\text{tp}} \cos\psi + A_{\text{ps}}^{\text{adh}} = F_{\text{ps}}, \tag{16}$$

$$A_{\text{ps}}^{\text{adh}} = 4\pi\gamma_L R_p + \frac{\bar{H}_{\text{ps}} R_p}{6a_0^2}, \tag{17}$$

where F_{ps} is the normal particle/substrate interaction force and F_{tp} is the tip/particle interaction force. These compressive forces cause deformations at the contact points between two objects that will be described in detail.

Also, F_{frict} is the nano friction force in the nanoparticle and the substrate interface. The proposed friction model will be presented in the next section. $\ddot{y}_p(t)$ is the discrete acceleration of the nanoparticle, $A_{\text{ps}}^{\text{adh}}$ is the adhesion force between the nanoparticle and the substrate and can be obtained by Eq. (15) [20,21], and γ_L is the liquid surface energy. A combination of the van der Waals and the capillary attractive forces are considered as the adhesion forces, and, for simplicity, no electrostatic force is assumed.

2.4. Contact mechanics

The tip/nanoparticle and nanoparticle/substrate interactions induce deformation on the contact surfaces. To model the contact elastic deformation, we use JKR contact mechanics [22-24]. JKR continuum contact mechanics includes effects of surface interactions between two contacting solid objects. The contact region radius, a, the contact area, A, and the penetration depth, δ, between the tip and the particle and also the particle and the substrate are given by:

$$A(t) = \pi(a^3)^{2/3} = \pi\Big\{\tilde{R}/K\Big[F(t) + 3\pi\tilde{R}\omega + \Big(6\pi\tilde{R}\omega F(t) + \Big(3\pi\tilde{R}\omega\Big)^2\Big)^{1/2}\Big]\Big\},$$

$$\delta = \frac{a^2}{\tilde{R}} - \frac{2}{3}\sqrt{\frac{3\pi\omega a}{K}},$$

$$K_{12} = \left[\frac{(1-\nu_1)^2}{E_1} + \frac{(1-\nu_2)^2}{E_2}\right],$$

$$\tilde{R} = R_1 R_2/(R_1 + R_2). \tag{18}$$

In the above equations, $F(t)$ is the normal force in the contact area. ω is the work of adhesion and for the two contact surfaces is obtained as [25]:

$$\omega_{12} = 2\sqrt{\gamma_1 . \gamma_2},$$

where γ is the surface energy. $\tilde{R}$ is the equivalent radius of the two contact surfaces, K is the equivalent elastic modulus of the two contact surfaces, and ν and E are Poisson ratio and Young's modulus.

2.5. Dynamic nano friction force

Unlike macroscopic friction, nano friction is velocity dependent, and stick-slip behavior is a major characteristic of nano friction [26,27]. Researchers have proposed the LuGre friction model to describe the observed phenomena in nanoscale [28,29]. The LuGre friction model exhibits a truly dynamical model which has been strongly analyzed and contains mathematical properties such as the existence and uniqueness of a solution and the boundedness of a solution [30].

The bristle deflection is presented as the state of the friction model. The bristle can be conceived as a cantilever rigidly connected to a body that deflects and slips through a terrain as the body is dragged across a surface. Figure 4 illustrates the schematic of the LuGre friction model.

In addition to having mentioned mathematical properties, the LuGre friction model also facilitates appropriate parameter tuning to obtain the friction response, as shown in Figure 5. In addition to slick-slip responses, a dependency on sliding velocity is another characteristic of the LuGre nano friction model.

The LuGre friction model will be used in this paper to characterize nano friction interaction between the nanoparticle and the substrate as follows [30,31]:

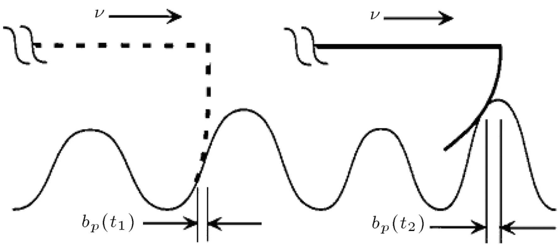

Figure 4. LuGre friction model [31].

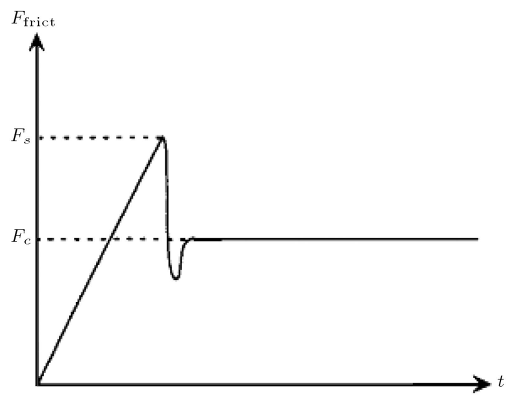

Figure 5. LuGre friction model response [31].

$$F_{\text{frict}} = \sigma_0 b_p(t) + \sigma_1(\dot{y}_p(t))\frac{db_p(t)}{dt} + F_\nu \dot{y}_p(t),$$

$$\frac{db_p}{dt} = \dot{y}_p - \frac{|\dot{y}_p|}{g(\dot{y}_p)} b_p,$$

$$g(\dot{y}_p) = \frac{1}{\sigma_0}\left[F_c + (F_s - F_c)e^{-(\dot{y}_p/\nu_s)^2}\right],$$

$$\sigma_1(\dot{y}_p) = \sigma_1 e^{-(\dot{y}_p/\nu_d)^2}, \qquad (19)$$

where $b_p(t)$ is bristle deflection, $\dot{y}_p(t)$ is the nanoparticle velocity along the manipulation direction, F_s and F_c are the static and kinetic friction magnitudes, respectively, σ_0 is bristle stiffness, σ_1 is the bristle damping coefficient, F_ν is the viscous damping coefficient, ν_s is the Stribeck velocity constant and ν_d is a velocity constant.

3. Controller design

This section is devoted to the design of an optimal sliding mode-based controller. The purpose of the controller is to maintain the tip at a constant height above the sample surface while the probe stage moves laterally, and the tip manipulates the target nanoparticle by exerting direct pushing force. The control scheme is illustrated in Figure 6.

3.1. Optimal sliding mode approach

Sliding mode control theory provides some essential tools to control systems with uncertainties or noise. The main problem with this method is that large amounts of control signal may be generated, which leads to control saturation or high energy expenditure. Consequently, optimizing this method may be useful.

Designing an optimal sliding surface for a time-invariant system has been studied by many researchers. In 1996, Koronodi et al. [4] designed an optimal

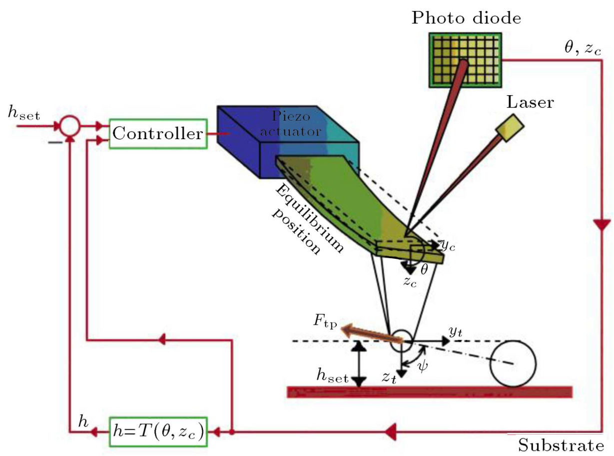

Figure 6. Control scheme for positioning the cantilever tip at a constant height above the sample substrate during lateral nanomanipulation.

sliding mode controller using the LQ method for a linear time invariant system. Tang and Misawa [32] used the LQR technique for sliding surface design. A linear sliding surface was utilized by both these papers. The designed optimal sliding surface in these references has two main characteristics: Firstly, it passes through the origin of phase space. Secondly, the slope of the surface is designed to optimize a desired cost function. Transforming this system to a regular form will divide the system into two separate parts; the control law appears explicitly in the first part, but not in the second part. So, the second part is an uncontrolled part and is known as the internal dynamics of a system. The slope of the sliding surface is designed based on internal dynamics, inasmuch as the stability of the overall system will be established by this part.

The transformation matrix, which transforms a system to an appropriate form such as a regular form, does not exist for all nonlinear systems. Hence, the choice of an optimal sliding surface is more complicated in nonlinear systems. Thus far, many methods have been developed to choose an optimal sliding surface for a nonlinear function. Zhou et al. [33] designed an optimal sliding-mode controller for guiding a homing missile to a maneuvering target. They considered target maneuvers as a system disturbance. So, sliding mode control provides them with a robust control strategy to reliably reach the target. In 2006, Nikkhah and Ashrafiuon [34] developed a method for optimal control of under-actuated systems. Bahrami et al. [35] also designed an optimal sliding mode controller for an aerospace application. Their main goal was to provide robustness against disturbances and increase terminal accuracy. In 2000, Salamci and Ozgoren [36] designed an optimal sliding mode controller for a missile autopilot by approximating the nonlinear system as a linear system.

In this study, the results of [36] are used to design optimal sliding surfaces for the main nonlinear system (Eqs. (7) to (9) and (14)). First, a linearization of the nonlinear system about an operating point, via the Taylor's series expansion method, is used to design the slope of the sliding surface. The linearized model does not obviously represent the global behavior of the original nonlinear system. Hence, the sliding controller which is modeled based on a linearized system, is suitable for a close neighborhood of the operating point. So, utilizing successive linearized models at operating points can extend the operating region of a sliding controller. Finally, control inputs which result from the linearized model are exerted to the nonlinear system [37,38].

3.2. *Optimal sliding mode controller design approach*

The nonlinear system of concern is represented by:

$$\frac{d}{dt}x = A(x)x + B(x)u, \qquad x \in R^n, \qquad u \in R^m, \tag{20}$$

where, $n = 8$ is the number of state variables and $m = 1$ is the number of control inputs. The states are θ, y_t, y_p, z_t and their derivatives. To design an optimal sliding surface, the system should be approximated as a sequence of linear time varying systems. For this purpose, it is linearized via the Taylor's series expansion method about each operating point, as follows [4,36]:

$$\frac{d}{dt}x = A(t)x + B(t)u, \qquad x \in R^n, \qquad u \in R^m. \tag{21}$$

This equation can be converted to the following form:

$$\frac{d}{dt}\begin{bmatrix} x_1 \\ x_2 \end{bmatrix} = \begin{bmatrix} A_{11} & A_{12} \\ A_{21} & A_{22} \end{bmatrix}\begin{bmatrix} x_1 \\ x_2 \end{bmatrix} + \begin{bmatrix} 0 \\ B_2 \end{bmatrix}u, \tag{22}$$

where $x_1 \in R^{n-m}$, $x_2 \in R^m$. The sliding surfaces can be written as:

$$s = x_2 + K_{\mathrm{LQ}}x_1 \qquad s \in R^m, \tag{23}$$

in which K_{LQ} should be specified as a design parameter. Indeed, different amounts of K_{LQ} cause different performances. In this work, the LQ method is used to determine K_{LQ} [4].

So, consider the subsystem:

$$\frac{d}{dt}x_1 = A_{11}x_1 + A_{12}x_2, \tag{24}$$

and the motion on the LQ optimal sliding surface minimizes the following cost function [6]:

$$J = \frac{1}{2}\int_0^t \{x_1(t)^T Q_1 x_1(t) + x_2(t)^T R_1 x_2(t)\}dt. \tag{25}$$

So, the K_{LQ} will be calculated from:

$$K_{\mathrm{LQ}} = R_1^{-1}A_{12}^T P, \tag{26}$$

in which $P > 0$ is the solution of the following Riccati equation:

$$PA_{11} + A_{11}^T P - PA_{12}R_1^{-1}A_{12}^T P + Q_1 + 0. \tag{27}$$

Now, to determine u_{eq}, $\dot{s}$ should be equal to zero.

$$\dot{s} = \dot{x}_2 + K_{\mathrm{LQ}}\dot{x}_1 = 0. \tag{28}$$

Control signal u_i $(i = 1 \dots m)$ equals:

$$u_i = u_{ieq} + M_i \mathrm{sat}\left(\frac{s_i}{\varphi}\right), \tag{29}$$

where M_i and φ are constant parameters. Using the Lyapunov function, $V = \frac{1}{2}s^T s$, we must be sure that:

$$s_i \dot{s}_i < 0. \tag{30}$$

In the following section, the proposed approach is applied to the nonlinear dynamics of the AFM. In this work, it is assumed that there is no uncertain parameter in the model.

4. Simulation results and discussion

Simulation of the nanomanipulation process after implementation of the designed controller is performed. The simulations include the manipulation of a gold-coated particle on a silicon oxide substrate by an AFM tip made of silicon. The chosen materials are widely used in experiments, so comparison can be made easily. The values of system parameters are listed in Table 1 [5,10,19,39,40].

For a nanomanipulation task, the AFM probe stage moves with a constant lateral velocity (V_{stage})

Table 1. System parameters values for simulation [5,10,19].

Symbol	Quantity	Value
	Geometry and mechanical parameters	
T	Microcantilever beam thickness	1×10^{-6} m
W	Microcantilever beam width	48×10^{-6} m
L	Microcantilever beam length	225×10^{-6} m
ρ	Microcantilever beam density	2330 kg/m^3
E	Microcantilever beam Young's modulus	169×10^9 Pa
ν	Microcantilever beam Poisson's ratio	0.27
H	AFM tip height	12×10^{-6} m
m_t	AFM tip mass	3×10^{-10} kg
I_t	AFM tip moment of inertia	23.4×10^{-22} kg.m^2
R_t	AFM Tip apex radius	25×10^{-9} m
R_p	Particle radius	150×10^{-9} m
ρ_p	Particle density	2230 kg/m^3
ν_t	Tip Poisson ratio	0.17
ν_P	Particle Poisson ratio	0.42
ν_S	Substrate Poisson ratio	0.16
E_t	Tip Young's modulus	135×10^9 Pa
E_P	Particle Young's modulus	3.8×10^9 Pa
E_S	Substrate Young's modulus	73×10^9 Pa
	Adhesion parameters	
γ_t	Tip surface energy	1.4 J/m^2
γ_p	Particle surface energy	1.5 J/m^2
γ_s	Substrate surface energy	0.16 J/m^2
a_0	Interatomic separation distance	3.75×10^{-10} m
$\bar{H}_{\text{tp}}$	Hamacker constant (Si-Water-Au) [39]	33.6×10^{-20} J
$\bar{H}_{\text{ps}}$	Hamacker constant (Au-Water-SiO$_2$) [40]	8.1×10^{-20} J
	Friction parameters	
F_S	Static friction magnitudes	1×10^{-9} N
F_C	Kinetic friction magnitudes	6×10^{-10} N
σ_0	Bristle stiffness	1×10^5 N/m
σ_1	Bristle damping coefficient	1.5×10^{-6} N.s/m
ν_s	Stribeck velocity constant	1×10^{-5} m/s
ν_d	Velocity constant	0.1 m/s
F_ν	Viscous damping coefficient	0 N.s/m
	Simulation parameters	
V_{stage}	Stage velocity	5×10^{-5} m/s
h_{set}	Desired tip center height	7.68×10^{-8} m
D_{set}	Initial horizontal distance of tip/particle centers	13.34×10^{-8} m

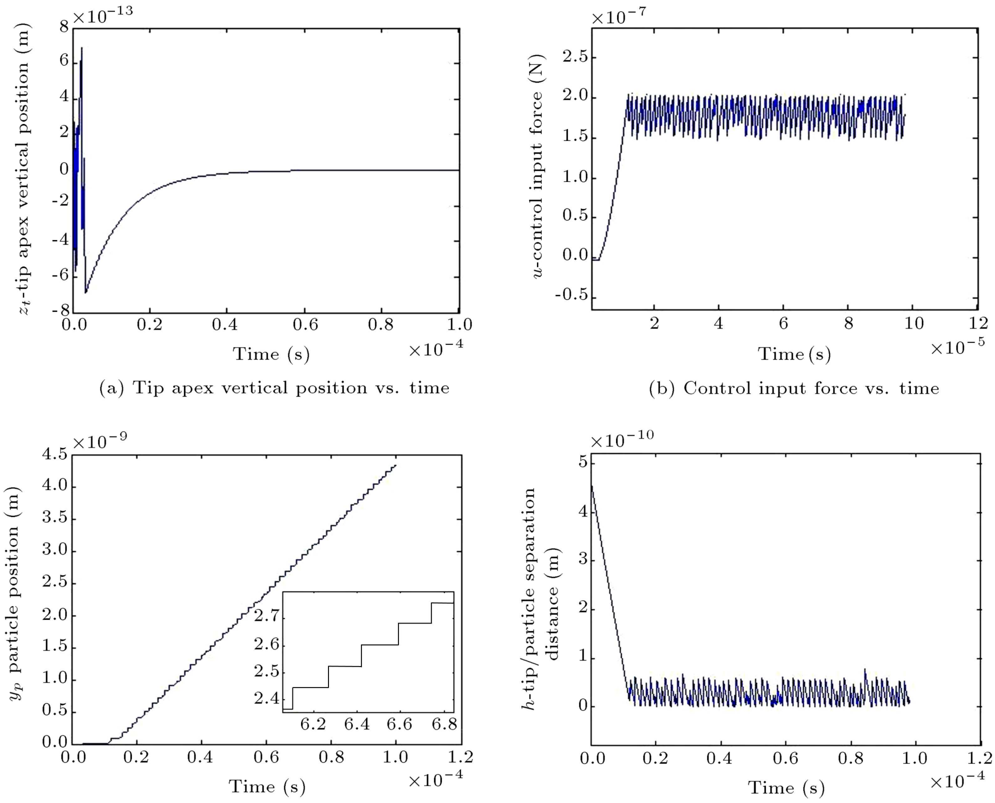

(a) Tip apex vertical position vs. time

(b) Control input force vs. time

(c) Particle position vs. time

(d) Tip/particle separation distance vs. time

Figure 7. Simulation results of nanoparticle manipulation by an AFM tip controlled using optimal sliding mode.

and approaches the target nanoparticle while the AFM tip is controlled to track a specified trajectory. The particle is supposed stationary on the substrate from the beginning. The separation distance between the tip-particle decreases gradually until the tip apex reaches the contact region with the particle and, then, the attractive interaction force between the tip-particle converts to a repulsive force. Due to the repulsive interaction force, the lateral deflection and torsional angle of the AFM tip increases, while the tip vertical position is controlled in order to remain at the horizontal line. Whenever the repulsive pushing force overcomes the LuGre friction force between the particle-substrate, the particle starts sliding on the substrate. It ceases again when the friction force becomes larger than the pushing force. The LuGre friction force is a function of the particle velocity and increases rapidly after particle movement. This stick-slip response repeats during the nanomanipulation task. Simulation of the nanoparticle manipulation is performed, while the controller is employed to control the AFM tip height. The simulation results have been shown over a short time for a better illustration of the parameters responses and behaviors. Nevertheless, the simulation results for a much longer simulation time showed the same bounded responses, as long as we keep the defined experiment conditions and simulation parameters constant.

Figure 7(a) depicts the tip apex vertical position versus time. As shown, the proposed controller maintains the tip apex on the desired trajectory, which is chosen as a horizontal line. The tracking simulation response shows that the tip has a slight undershoot and then returns to the desired line with an acceptable resolution. The input force signal is depicted in Figure 7(b), and it is shown to be bounded. It initially jumps to an approximately constant value, and fluctuates about this value when the system reaches a steady-state behavior and the tip-particle remains in the contact mode.

The particle position versus time is depicted in Figure 7(c). Initially, the nanoparticle stays motionless and then moves with a stick-slip behavior on the substrate in the y-axis direction, as shown in Figure 7(c). This figure indicates that the particle periodically experiences a positive and negative acceleration. During the particle stick-slip motion, the particle has positive acceleration while the pushing force is dominant over the friction force, and it has negative acceleration when the friction force becomes larger. The average velocity of the nanoparticle is about 0.5 μm/s, which is equal to the velocity of the probe stage.

Figure 7(d) shows the separation distance between the external surfaces of the particle-tip after nanoscale deformation. As shown, the parameter decreases until it reaches the contact region, according to the Derjaguin interaction model, and after that, the nanoparticle starts to move. This parameter fluctuates around a constant value of about 21 Angstrom. During the particle stick-slip motion, the separation distance increases while the particle slides on the substrate and decreases when the particle is in the sticking phase.

By solving the Riccati equation for $P > 0$, optimal sliding mode coefficients ($K_{\mathrm{LQ}i}(i = 1 \cdots 7)$) can be calculated from Eq. (25), as shown in Figure 8(a)-(d). These figures show that the slopes of the optimal sliding surface are tuned after a while, and then, they reach a smaller and constant value. Table 2 shows their final values. Figure 8(b) and (c) show that K_3, K_4 and K_5 are larger than other coefficients. These coefficients correspond to the y_p, z_t and $\dot{\theta}$ states. Consequently, they are the chief states in the optimal sliding mode controller design.

Table 2. Final values of K_{LQ}.

Final	K_1	K_2	K_3	K_4	K_5	K_6	K_7
values	540.3	340.3	9302	8271.8	12030.1	12.3	0.03

Contact deformations between the tip-particle and the particle-substrate are obtained using a JKR contact mechanics model, and are depicted in Figure 9. The tip-particle penetration depth is presented in Figure 9(a). The graph has an initial jump, which corresponds to the tip-particle approaching time, and when the tip approaches and remains in the contact region with the particle, the graph shows a stick-slip pattern. The particle-substrate penetration depth on the contact surface is also given in Figure 9(b). The profile similarly shows an initial jumping and follows a stick-slip pattern with increasing and decreasing amplitude, with respect to time.

5. Conclusion

An optimal sliding mode approach is applied to the AFM probe in order to control and suppress the

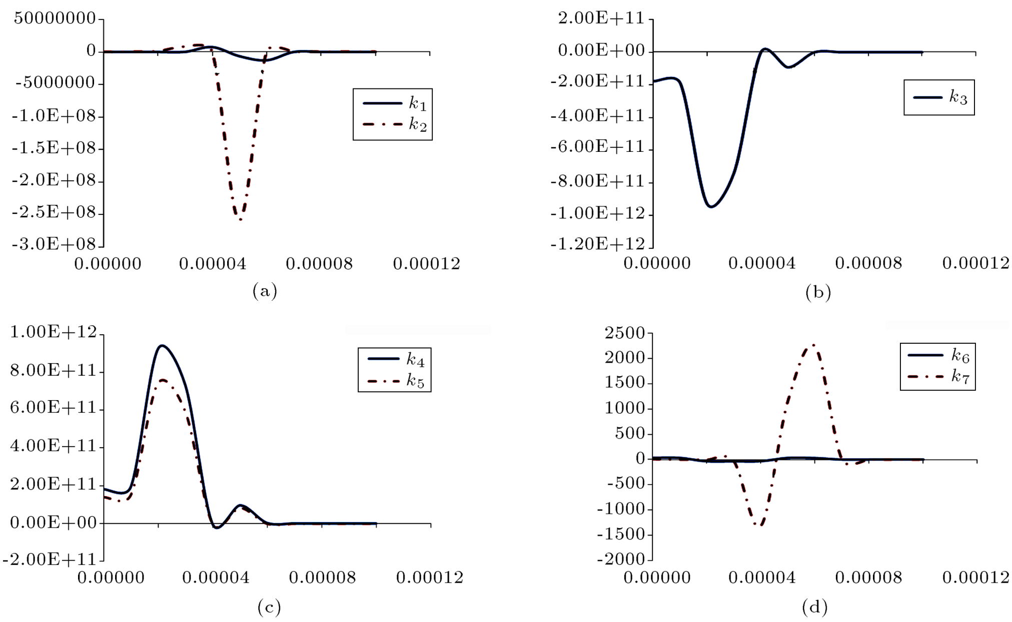

Figure 8. Optimal sliding mode coefficients over time ($K_{\mathrm{LQi}}(i = 1 \cdots 7)$).

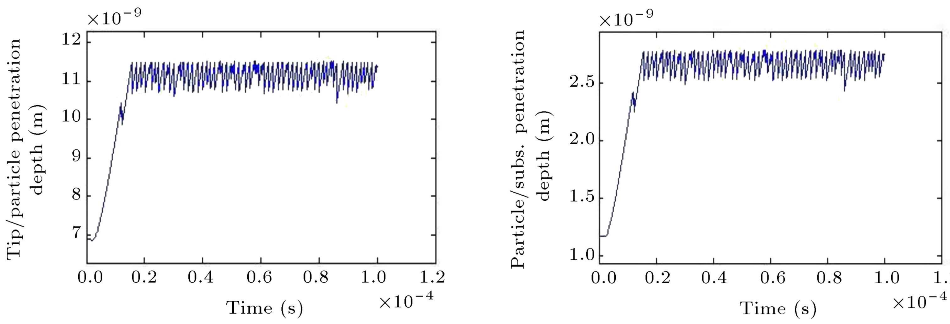

(a) Tip/particle penetration depth vs. time

(b) Particle/substrate penetration depth vs. time

Figure 9. Contact deformations results of the nanomanipulation simulation.

vibration behavior of the AFM microcantilever for a 2-D lateral nanomanipulation task. In this paper, a complete model of the pushing based manipulation of a nanoparticle by an AFM probe is presented. The proposed nanomanipulation model is divided into the AFM probe and the nanoparticle dynamics, and consists of all effective phenomena in the nanoscale. Nanoscale interaction forces, elastic deformation in contact areas, and dynamic friction force are considered in the tip-particle-substrate system model. The proposed dynamic friction model depends on the relative velocity and produces the stick-slip behavior of the nanoparticle.

The optimal sliding mode control approach provided good performance with a simple control structure. In this control approach, slope tuning of the sliding surface is chosen using the LQ method in order to optimize the cost function. First, a successive approximation approach is used to approximate the main nonlinear system as a linear time variant system at each operating point. Then, the LQ method is used to design the control input for approximated systems. The control input which is generated from the approximated system is applied to the original nonlinear system. The simulation results showed that the proposed controller law can track the desired trajectory with perfect accuracy.

References

1. Delnavaz, A., Jalili, N. and Zohoor, H. "Vibration control of AFM tip for nano-manipulation using combined sliding mode approach", *7th IEEE Int. Conf. on Nanotechnology*, Hong Kong, China, pp. 106-111 (2007).
2. Sitti, M. and Hashimoto, H. "Controlled pushing of nanoparticles: Modeling and experiments", *IEEE/ASME Trans. on Mechatron.*, **5**(2), pp. 199-211 (2000).
3. El Raifi, K., El Raifi, O. and Toumi, K.Y. "Modeling and control of AFM-based nano-manipulation systems", *IEEE Int. Conf. on Robotics and Automation*, Barcelona, Spain, pp. 157-162 (2005).
4. Koronodi, P., Hashimoto, H., Gajdar, T. and Suto, Z. "Optimal sliding mode design for motion control", *IEEE Int. Symp. on Industrial Electronics*, Warsaw, Poland, **1**, pp. 277-282 (1996).
5. Tafazzoli, A. and Sitti, M. "Dynamic behavior and simulation of nanoparticle, sliding during nanoprobe-based positioning", *IMECE/ASME Int. Mechanical Eng. Congress & Exposition*, Anaheim, CA, pp. 965-972 (2004).
6. Tafazzoli, A., Pawashe, C. and Sitti, M. "Atomic force microscope based two-dimensional assembly of micro/nanoparticles", *IEEE Conf. on Nanotechnology*, Montreal, Canada, pp. 230-235 (2005).
7. Tafazzoli, A. and Sitti, M. "Dynamic modes of nanoparticle motion during nanoprobe based manipulation", *IEEE Conference on Nanotechnology*, Munich, Germany (2004).
8. Korayem, M.H. and Zakeri, M. "Sensitivity analysis of nanoparticles pushing critical conditions in 2-D controlled nanomanipulation based on AFM", *Int. J. Manuf. Tech.*, **41**, pp. 714-726 (2008).
9. Zhou, Q., Kallio, P., Aria, F., Fukuda, T. and Koivo, K.N. "A model for operating spherical micro objects", *10th Int. Symp. on Micro-mechatronics and Human Science*, Nagoya-shi, Japan, pp. 79-85 (1999).
10. Mualim, Y., Ghorbel, F. and Dabney, J.B. "AFM nano-manipulation modeling and simulation", *IMECE/ASME Int. Mechanical Eng. Congress & Exposition*, Chicago, IL, USA (2006).
11. Landolsi, F., Ghorbel, F.H. and Dabney, J.B. "An AFM-based nanomanipulation model describing the atomic two dimensional stick-slip behavior", *IMECE/ASME Int. Mechanical Eng. Congress & Exposition, Seattle*, WA, USA, pp. 177-186 (2007).
12. Mahboobi, S.H., Meghdari, A., Jalili, N. and Amiri, F. "Two-dimensional atomistic simulation of metallic nanoparticles pushing", *Mod. Phys. Lett. B*, **23**(22), pp. 2695-2702 (2008).
13. Mahboobi, S.H., Meghdari, A., Jalili, N. and Amiri, F. "Qualitative study of nanocluster positioning process: Planar molecular dynamics simulations", *Curr. Appl. Phy.*, **9**(5), pp. 997-1004 (2009).
14. Jalili, N., Dadfarnia, M. and Dawson, D.M. "A fresh insight into the microcantilever-sample interaction problem in non-contact atomic force microscopy", *ASME J Dyn. Syst., Meas., Control*, **126**(2), pp. 327-335 (2004).
15. Ashhab, M., Salapaka, M.V., Dahleh, M. and Mezic, I. "Dynamic analysis and control of microcantilevers", *Automatica*, **35**(10), pp. 1663-1670 (1999).
16. Sitti, M. and Hashimoto, H. "Macro to nano tele-manipulation through nanoelectromechanical systems", *24th IEEE Industrial Electronics Society Annual Conf.*, Aachen, Germany, **1**, pp. 98-103 (1998).
17. Saeidpourazar, R. and Jalili, N. "Towards fused vision and force robust feedback control of nanorobotic-based manipulation and grasping", *Mechatronics*, **18**(10), pp. 566-577 (2008).
18. Stark, R.W., Schitter, G. and Stemmer, A. "Tuning the interaction forces in tapping mode atomic force microscopy", *Physical Review B*, **68**, 085401 (2003).
19. Sitti, M. "Atomic force microscope probe based controlled pushing for nanotribological characterization", *IEEE/ASME Transactions on Mechatronics*, **9**(2), pp. 343-349 (2004).
20. Tian, X., Wang, Y., Xi, N. and Dong, Z. "A study on theoretical nano forces in AFM based nanomanipulation", *2nd IEEE Int. Conf. on Nano/Micro Engineered and Molecular Systems*, Bangkok, Thailand, pp. 917-921 (2007).

21. Yang, Q. and Jagannathan, S. "Nanomanipulation using atomic force microscope with drift compensation", *IEEE American Control Conf.*, Minneapolis, MN, USA, pp. 514-519 (2006).

22. Bhushan, B., *Introduction to Tribology*, John Wiley and Sons, New York (2002).

23. Israelachili, J., *Intermolecular and Surface Forces*, 2nd Ed., Academic Press London (1992).

24. Johnson, K.L., *Contact Mechanics*, Cambridge University, London (1985).

25. Jalili, N., Dadfarnia, M. and Dawson, D.M. "A fresh insight into the microcantilever-sample interaction problem in non-contact atomic force microscopy", *ASME J. Dynamic Syst. Meas. Control*, **126**, pp. 327-35 (2004).

26. Falvo, M.R., Taylor, R.M., Helser, A., Chi, V., Brooks, F.P., Washburn, S. and Superfine, R. "Nanometer-scale rolling and sliding of carbon nanotubes", *Nature*, **397**, pp. 236-238 (1999).

27. Braiman, Y., Family, F. and Hentschel, H.G.E. "Nonlinear friction in the periodic stick-slip motion of coupled oscillators", *Phys. Rev. B*, **55**, pp. 5491-5504 (1997).

28. Meurk, A. "Microscopic stick-slip in friction force microscopy", *Tribol. Lett.*, **8**, pp. 161-169 (2000).

29. Stark, R.W., Schitter, G. and Stemmer, A. "Velocity dependent friction laws in contact mode atomic force microscopy", *Ultramicroscopy*, **100**, pp. 309-317 (2004).

30. Olsson, H. "Control systems with friction", Dissertation, Lund Institute of Technology (1996).

31. Mualim, Y. "Nanomanipulation modeling and simulation", Master's Thesis, Rice University (2007).

32. Tang, C.Y. and Misawa, E.A. "Sliding surface design for discrete VSS using LQR technique with a present real eigenvalues", *IEEE American Control Conference*, San Diego, CA, USA (1999).

33. Zhou, D., Chundi, M., Ling, Q. and Xu, W. "Optimal sliding mode guidance of homing missile", *38th IEEE Conf. on Decision and Control*, Phoenix, AZ, USA, **5**, pp. 5131-5136 (1999).

34. Nikkhah, M. and Ashrafiun, H. "Optimal sliding mode control for underactuated systems", *IEEE American Control Conf.*, Minneapolis, MN, USA (2006).

35. Bahrami, M., Ebrahimi, B. and Roshanian, J. "Optimal sliding-mode guidance law for fixed interval propulsive maneuvers", *IEEE Int. Conf. on Control Applications*, Munich, Germany, pp. 1014-1018 (2006).

36. Salamci, M.U. and Ozgoren, M.K. "Sliding mode control with optimal sliding surfaces for missile autopilot design", *J. Guid. Control Dyn.*, **23**(4), pp. 719-727 (2000).

37. Yeh, F.K., Chein, H.S. and Chen, L. "Design of optimal midcourse guidance sliding-mode control for missiles with TVC", *IEEE Transactions on Aerospace and Electronic Systems*, **39**(3), pp. 824-837 (2003).

38. Novin Zade, A. "Closed loop optima-fuzzy control in nonlinear systems", Dissertation, Sharif University of Technology (2005).

39. Rollot, Y., Regnier, S. and Guinot, J.C. "Simulation of micro-manipulation: Adhesion forces and specific dynamic models", *Int. J. Adh. & Adh.*, **19**, pp. 35-48 (1999).

40. De Wit, C., Olsson, H., Astrom, K.J. and Lischinsky P. "A new model for control of systems with friction", *IEEE Trans. Automatic Control*, **40**(3), pp. 419-25 (1995).

Biographies

Hesam Babahosseini received his BS degree from the International University of Imam Khomeini, Qazvin, Iran, in 2007, and his MS degree from Sharif University of Technology, Tehran, Iran, in 2010, both in Mechanical Engineering. He is currently working towards a PhD degree in Mechanical Engineering in the Virginia Tech Microelectromechanical Systems Laboratory at the Bradley Department of Electrical and Computer Engineering, Virginia Polytechnic Institute and State University, Blacksburg, USA.

His research interests include bioMEMS, microfluidics, micro-fabrication, and AFM with applications in cellular biomechanics and mechanobiology investigations.

Seyed Hanif Mahboobi received his BS, MS and PhD degrees in Mechanical Engineering, in 2002, 2004 and 2009, respectively, from Sharif University of Technology, where he was also a member of the Center of Excellence in Design, Robotics, and Automation (CEDRA). He then attended the Institute for Nanoscience and Nanotechnology (INST) as a postdoctoral researcher. He is currently a postdoctoral researcher at the California Institute for Quantitative Biosciences at UC Berkeley, USA. His research interests include robotics, nanomanipulation, computational nanoscience and biomolecular simulation.

Majid Khorsand Vakilzadeh received his BS and MS degrees in Mechanical Engineering from Amirkabir University and Sharif University of Technology, respectively, and is currently pursuing his PhD degree in the Department of Applied Mechanics at Chalmers University of Technology, Sweden. His research is focused on structural dynamics, model order reduction and stochastic finite element model updating.

Aria Alasty received his BS and MS degrees in Mechanical Engineering from Sharif University of Technology (SUT), Tehran, Iran, in 1987 and 1989, respectively, and a PhD degree in from Carleton University, Ottawa, Canada, in the same subject, in 1996. He is currently Professor of Mechanical Engineering in Sharif University of Technology, and has been a member of the Center of Excellence in Design, Robotics, and Automation (CEDRA) since 2001. His fields of research are mainly in nonlinear and chaotic systems control, computational nano/micro mechanics and control, special purpose robotics, robotic swarm control, and fuzzy system control.

Ali Meghdari received his PhD degree in Mechanical Engineering from the University of New Mexico in 1987, and then collaborated with the robotics group of the Los Alamos National Laboratory (LANL) as a postdoctoral research fellow. From 1996-1999 he chaired the School of Mechanical Engineering at Sharif University of Technology, Tehran, Iran. From 2001-2010, he also served as Provost and Vice-President of Academic Affairs at the university and is currently Director of the Center of Excellence in Design, Robotics and Automation (CEDRA), and in 1997 was granted the rank of professor, and was recognized by the Iranian Society of Mechanical Engineers (ISME) as the youngest (at age 37) ME full-professor in Iran. During 1993-94, he was a visiting research faculty at the AHMCT center of the University of California-Davis, and from 1999-2000, he served the IBDMS and RMMRL research centers of the Colorado School of Mines as a visiting research professor.

Dr. Meghdari has performed extensive research in the areas of robotics kinematics/dynamics, nano-manipulations and modeling of biomechanical systems. He has published over 220 technical papers in refereed international journals and conferences, and supervised numerous MS and PhD dissertations. He has also been the recipient of various scholarships and awards. He is on the editorial board of various engineering journals, and an affiliate member of the Iranian Academy of Sciences (IAS), the latest being: the 2012 Allameh Tabatabee Distinguished Professorship Award for Excellence in Teaching and Research by the National Elite Foundation of Iran. He is a fellow of the ASME (American Society of Mechanical Engineers).